HYPERSPECTRAL IMAGE UNMIXING VIA QUADRATIC PROGRAMMING

Zhuocheng Yang and James Farison

Baylor University
Department of Electrical & Computer Engineering

1. INTRODUCTION

Hyperspectral image unmixing has received considerable interest in remote sensing image processing due to the significantly improved spectral resolution by recent advances in hyperspectral sensing instruments. The need for hyperspectral image unmixing in remotely sensed imagery arises from the fact that the sampling distance is generally larger than the size of the targets of interest. For example, NASA's AVIRIS imaging system has a spatial resolution of 20 meters when flying at 20 kilometers above sea level. Under this circumstance, it is likely that a pixel area is occupied by more than one material. Two mixture models have been proposed to represent the synthesis of the mixed pixels. One is a linear model that considers a mixed spectrum as a linear combination of endmember spectra present in the pixel area weighted by fractional area coverage [1]. The other is a nonlinear model [2]. As the linear model is the most frequently used model for studying material quantification, we consider only the linear model in this paper.

Assume that there are L spectral bands and that $\boldsymbol{r}$ is an L-dimensional pixel vector. Suppose there are p ($p < L$) distinct endmembers present in the pixel area and their spectra are $\boldsymbol{m_1}, \boldsymbol{m_2}, \ldots, \boldsymbol{m_p}$, respectively. The fraction of each endmember is specified by the values $\alpha_1, \alpha_2, \ldots, \alpha_p$. The linear mixture model can be expressed as follows:

$$\boldsymbol{r} = \sum_{i=1}^{p} \alpha_i \boldsymbol{m_i} + \boldsymbol{n} = M\boldsymbol{\alpha} + \boldsymbol{n} \tag{1}$$

where $M = [\boldsymbol{m_1}, \boldsymbol{m_2}, \ldots, \boldsymbol{m_p}]$, $\boldsymbol{\alpha} = [\alpha_1, \alpha_2, \ldots, \alpha_p]^T$, and $\boldsymbol{n}$ represents additive noise.

To be physically meaningful, the nonnegativity constraint requires all abundances to be nonnegative such that $\alpha_i \geq 0$ for all $1 \leq i \leq p$. A few papers in the literature also incorporate another physical constraint, known as the sum-to-one constraint when estimating endmember fractions [3, 4, 5]. The sum-to-one constraint demands $\sum_{i=1}^{p} \alpha_i = 1$. Nevertheless, this condition is strictly valid for the situation where the endmembers are arranged on the surface in a segregted manner, which is almost never satisfied in reality [6]. As a result, a method specifically designed for the sum-to-one constraint can easily become vulnerable when the sum-to-one condition does not remain valid. In this paper, we relax the sum-to-one constraint as we develop our estimation approach. The sum of the estimated fractions in every pixel is bound to a range rather than being fixed on the value of one. From now on, we call it the relaxed sum-to-one constraint. In Section 2, we replace the sum-to-one constraint with the relaxed sum-to-one constraint and develop a least squares solution via quadratic programming, which has been demonstrated applicable to linear unmixing in our previous work [5]. Computer simulations are offered in Section 3 to show that fully constrained methods can become incompetent due to a slight variation in the sum of the fractions and that our method with relaxed sum-to-one constraint is superior to the fully constrained methods in terms of variation.

2. UNMIXING WITH NONNEGATIVITY AND RELAXED SUM-TO-ONE CONSTRAINTS

The hyperspectral image unmixing problem can be formulated as the following optimization problem:

$$\text{Minimize } f(\boldsymbol{\alpha}) = (\boldsymbol{r} - M\boldsymbol{\alpha})^T(\boldsymbol{r} - M\boldsymbol{\alpha}) = \boldsymbol{\alpha}^T\boldsymbol{M}^T M\boldsymbol{\alpha} - 2\boldsymbol{r}^T\boldsymbol{M}\boldsymbol{\alpha} + \boldsymbol{r}^T\boldsymbol{r} \tag{2}$$

The relaxed sum-to-one constraint (RSC) and nonnegativity constraint (NC) have the following forms:

$$RSC : l \leq \boldsymbol{E}\boldsymbol{\alpha} \leq h \quad \text{and} \quad NC : -B\boldsymbol{\alpha} \preceq \boldsymbol{0} \tag{3}$$

where the p-dimensional vector $\boldsymbol{E} = [1, 1, \ldots, 1]$, B is a $p \times p$ identity matrix, and p is the number of the endmembers present in the pixel area. The inequality symbol $\preceq$ in Equation (3) represents componentwise inequality. The lower bound l and upper

bound h define the box constraint imposed on the abundance fractions. Combining the two constraints, we can get the inequality functions $F\boldsymbol{\alpha} \preceq \boldsymbol{d}$, where $F = \begin{bmatrix} -B \\ E \\ -E \end{bmatrix}$ and $\boldsymbol{d} = \begin{bmatrix} \mathbf{0} \\ h \\ l \end{bmatrix}$. The barrier method [7], a particular algorithm to quadratic programming problem, puts the inequality constraint into the objective function by the logarithmic barrier function $\sum_{i=1}^{p} -\frac{1}{t}\log(\boldsymbol{F_i}^T\boldsymbol{\alpha})$, where $\boldsymbol{F_i}^T$ is the ith row of F. The final form is:

$$\text{Minimize } f(\boldsymbol{\alpha}) = \boldsymbol{\alpha}^T M^T M\boldsymbol{\alpha} - 2\boldsymbol{r}^T M\boldsymbol{\alpha} + \boldsymbol{r}^T\boldsymbol{r} + \sum_{i=1}^{p} -\frac{1}{t}\log(\boldsymbol{F_i}^T\boldsymbol{\alpha}) \tag{4}$$

The logarithmic barrier function is an approximation to the indicator function. As t grows, the quality of the approximation improves [7]. Newton's method can find the estimate by gradually increasing the value of t. The estimate obtained from each iteration is used as the starting point for the next iteration. The details of our method are given in Algorithm 1. The Newton step $\boldsymbol{\Delta\alpha}$ and Newton decrement λ are determined by $-\nabla^2 f(-\boldsymbol{\alpha}^{(k)})^{-1}\nabla f(\boldsymbol{\alpha}^{(k)})$ and $\left[(\boldsymbol{\Delta\alpha}^{(k)})^T\nabla^2 f(\boldsymbol{\alpha}^{(k)})\boldsymbol{\Delta\alpha}^{(k)}\right]^{-\frac{1}{2}}$, and p is the number of the distinct endmembers.

Algorithm 1 Hyperspectral image unmixing

Initialize parameters t, $\boldsymbol{\alpha}^{(1)}$, μ, ϵ, ϵ_{Newton}
$k = 1$
while $p/t > \epsilon$ **do**
  Compute the Newton step $\boldsymbol{\Delta\alpha}^{(k)}$ and the decrement λ
  while $\lambda > \epsilon_{Newton}$ **do**
    Find step size τ by backtracking line search
    $\boldsymbol{\alpha}^{(k)} = \boldsymbol{\alpha}^{(k)} + \tau\boldsymbol{\Delta\alpha}^{(k)}$
    Compute the Newton step $\boldsymbol{\Delta\alpha}^{(k)}$ and the decrement λ
  end while
  $t = \mu t$
  $\boldsymbol{\alpha}^{(k+1)} = \boldsymbol{\alpha}^{(k)}$, $k = k + 1$
end while
$\hat{\boldsymbol{\alpha}} = \boldsymbol{\alpha}^{(k)}$

3. EXPERIMENTAL RESULTS

In this section, we demonstrate a comparative analysis among OSP [8], QPFCLS [5], and our approach. The first two approaches are selected to represent the unconstrained and fully constrained approaches, respectively. A set of reflectance spectra is selected from the USGS Digital Spectral Library [9]. The set contains seven spectra: maple leaf, blackbrush, pinon pine, aspen leaf, saltbrush, azurite, and sagebrush. Their spectra are shown in Figure 1. In this example, 1000 mixed pixels are simulated. The fraction of each endmember is illustrated in Figure 2.

3.1. Sum-to-one condition strictly satisfied

The sum of the fractions in each pixel is set to one to comply strictly with the sum-to-one condition. White Gaussian noise is added to every spectral band to achieve the SNR of 30:1. The SNR is defined as $\frac{1}{L}\sum_{i=1}^{L}\lambda_i$, where L is the number of the bands and λ_i is the SNR of the ith band, defined as 50% averaged reflectance in the ith band divided by the standard deviation of the noise. Figure 3 displays the fraction estimations of saltbrush, which is only added to pixel numbers 400–600 with 10% fraction. The root mean square (RMS) errors are calculated to measure the similarity between the true and estimated fractions. The RMS errors of the seven materials are tabulated in Table 1. We find QPFCLS produces the best estimates. However, this is not the case when we add variations to the fraction vectors.

3.2. Sum-to-one condition not satisfied

In this example, we add variations to the fraction vectors by multiplying each fraction vector by a random variable $\boldsymbol{x}$, where $\boldsymbol{x} \sim \mathcal{N}(\mu, \sigma^2)$. We set μ and σ to be 1 and 0.0304, respectively. The fraction vector that we are trying to estimate in each

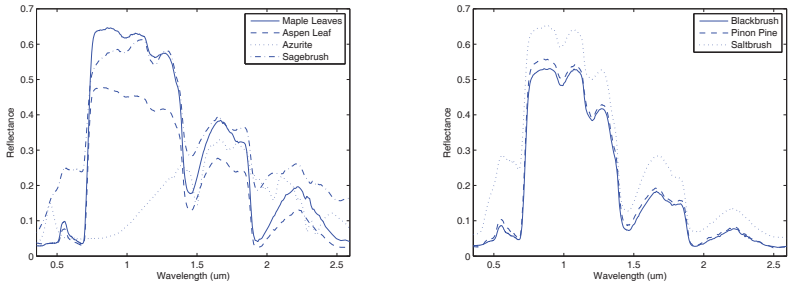

(a) (b)

Fig. 1: Reflectance spectra.

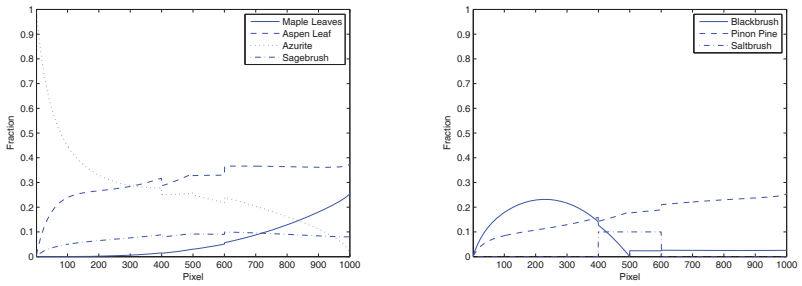

(a) (b)

Fig. 2: Simulated fractions.

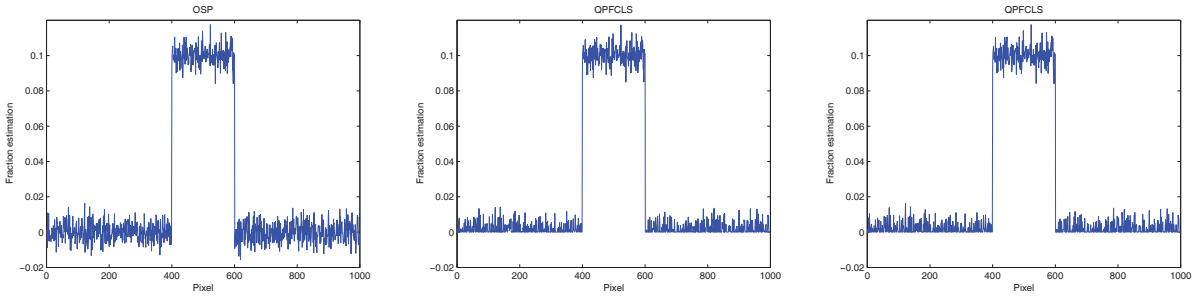

(a) OSP (b) QPFCLS (c) Our Approach

Fig. 3: Estimation results of saltbrush obtained by OSP, QPFCLS, and our approach when sum-to-one condition is satisfied.

Table 1: Root mean square errors of seven materials when sum-to-one condition is satisfied.

Approach	Maple leaf	Blackbrush	Sagebrush	Aspen leaf	Azurite	Pinon pine	Saltbrush
OSP	1.486×10^{-2}	2.690×10^{-2}	5.709×10^{-3}	1.985×10^{-2}	4.382×10^{-3}	2.992×10^{-2}	5.229×10^{-3}
QPFCLS	6.378×10^{-3}	2.242×10^{-2}	4.648×10^{-3}	1.295×10^{-2}	3.534×10^{-3}	2.647×10^{-2}	3.956×10^{-3}
Our approach	1.304×10^{-2}	2.423×10^{-2}	4.777×10^{-3}	1.795×10^{-2}	4.292×10^{-3}	2.712×10^{-2}	3.970×10^{-3}

pixel becomes $\boldsymbol{\alpha}_{New} = \boldsymbol{x}\boldsymbol{\alpha}$. The lower and upper bounds used in the relaxed sum-to-one constraint are selected to be 0.9 and 1.1. Estimation results of saltbrush and RMS errors of the seven materials are illustrated in Figure 4 and Table 2. Apparently, QPFCLS, a fully constrained approach, has an enormous degradation in estimation performance, while our approach performs the best in this case.

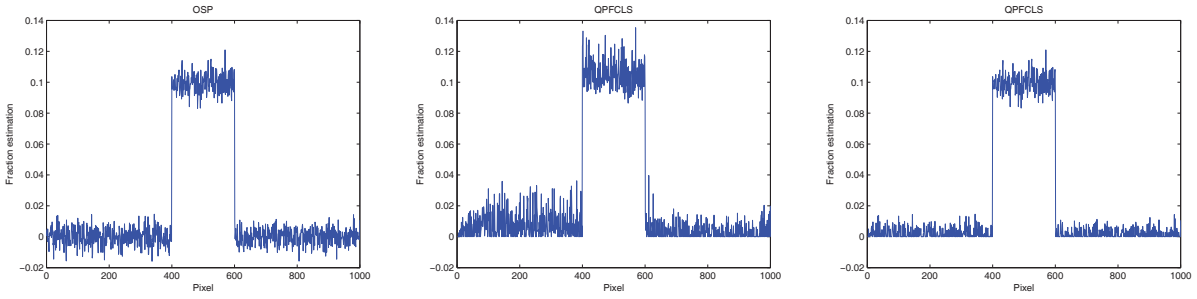

(a) OSP (b) QPFCLS (c) Our Approach

Fig. 4: Estimation results of saltbrush obtained by OSP, QPFCLS, and our approach when sum-to-one condition is not satisfied.

Table 2: Root mean square errors of seven materials when sum-to-one condition is not satisfied.

Approach	Maple leaf	Blackbrush	Sagebrush	Aspen leaf	Azurite	Pinon pine	Saltbrush
OSP	1.500×10^{-2}	2.644×10^{-2}	5.951×10^{-3}	1.984×10^{-2}	4.232×10^{-3}	2.887×10^{-2}	5.439×10^{-3}
QPFCLS	4.821×10^{-2}	4.496×10^{-2}	1.801×10^{-2}	5.383×10^{-2}	2.198×10^{-2}	3.472×10^{-2}	9.754×10^{-3}
Our approach	1.285×10^{-2}	2.335×10^{-2}	4.956×10^{-3}	1.749×10^{-2}	4.030×10^{-3}	2.574×10^{-2}	4.239×10^{-3}

4. CONCLUSION

The relaxed sum-to-one constraint is proposed in this paper, and a comparative analysis is provided to demonstrate that the fully constrained unmixing approach can become vulnerable for the situation where the sum-to-one condition is not strictly met. The approach suggested by our paper, incorporating the nonnegativity and relaxed sum-to-one constraints are more capable of unmixing problems when sum-to-one condition is not satisfied, which always occurs in reality.

5. REFERENCES

[1] R. B. Singer and T. B. McCord, "Mars: Large scale mixing of bright and dark surface materials and implications for analysis of spectral reflectance," in *10th Lunar and Planetary Science Conference*, New York, March 1979, pp. 1835–1848.

[2] B. Hapke, "Bidirection reflectance spectrocopy. I. theory," *Journal of Geophysical Research*, vol. 86, pp. 3039–3054, April 1981.

[3] D. C. Heinz and Chein-I-Chang, "Fully constrained least squares linear spectral mixture analysis method for material quantification in hyperspectral imagery," *IEEE Transactions on Geoscience and Remote Sensing*, vol. 39, no. 3, pp. 529–545, Mar 2001.

[4] C. I. Chang, H. Ren, C. C. Chang, F. D'Amico, and J. O. Jensen, "Estimation of subpixel target size for remotely sensed imagery," *IEEE Transactions on Geoscience and Remote Sensing*, vol. 42, no. 6, pp. 1309–1320, 2004.

[5] Z. Yang, J. Farison, and M. Thompson, "Fully constrained least squares estimation of target quantifications in hyperspectral images," in *IPCV*, 2009, pp. 910–915.

[6] N. Keshava and J. F. Mustard, "Spectral unmixing," *IEEE Signal Processing Magazine*, vol. 19, no. 1, pp. 44–57, January 2002.

[7] S. P. Boyd and L. Vandenberghe, *Convex Optimization*, Cambridge University Press, Cambridge, 2004.

[8] C. I. Chang, "Orthogonal subspace projection (OSP) revisited: A comprehensive study and analysis," *IEEE Transactions on Geoscience and Remote Sensing*, vol. 43, no. 3, pp. 502–518, 2005.

[9] R. N. Clark, G. A. Swayze, R. Wise, E. Livo, T. Hoefen, R. Kokaly, and S. J. Sutley, "USGS digital spectral library splib06a: U.S. geological survey," 2007.